Case Studies in Construction Materials 16 (2022) e00957

Contents lists available at ScienceDirect

Case Studies in Construction Materials

journal homepage: www.elsevier.com/locate/cscm

Model updating of a masonry tower based on operational modal analysis: The role of soil-structure interaction

Amirhosein Shabani *, Mohyeddin Feyzabadi, Mahdi Kioumarsi

Department of Civil Engineering and Energy Technology, Oslo Metropolitan University, Oslo 0166, Norway

ARTICLE INFO

Keywords:
Digital twins
Model updating
Soil-structure interaction
Masonry tower
Operational modal analysis
Resonance effect

ABSTRACT

Vibration-based finite element model (FEM) updating of cultural heritage assets is gaining so much attraction these days since destructive tests are usually not allowed to be performed. In this study, a framework for developing three-dimensional (3D) FEMs is proposed using 3D laser scanners and applied on Slottsfjell tower, a stone masonry tower in Tønsberg, Norway. Operational modal analysis (OMA) was done based on the ambient vibration testing (AVT) data to define the frequency values and corresponding mode shapes of the tower. Mechanical properties of the tønsbergite stone were utilized to derive the base values of the material properties of the homogenized masonry for performing sensitivity analysis and FEM updating. To investigate the effect of the soil-structure interaction (SSI) on the FEM updating results, three FEMs are developed. The fixed-base model is the FEM without considering the SSI effects, and two other FEMs are developed using the substructure and direct methods for simulating the SSI effects. Sensitivity analysis was performed to investigate the effective parameters on the dynamic characteristics of the models. FEM updating was conducted on the three FEMs, and results are compared to each other to show the role of the SSI on the FEM updating results. The resonance effect can cause damages to buildings located even in low seismicity zones. For this aim, the risk of resonance effect has been evaluated for the tower. Finally, linear dynamic analysis was performed on the three calibrated models, and the results were compared to each other.

1. Introduction

Heritage structures are the symbolic representation of ancient engineering, and preservation of the so-called architectural heritage is pivotal for every societies [1]. Masonry and timber are considered as the oldest construction materials [2]. The structural behavior of masonry structures is strictly tied to the geometrical parameters, material properties, and environmental situation of the location site [3,4]. Moreover, providing a robust model called digital twins with a structural behavior similar to the real structure is crucial for a structural vulnerability assessment methodology [5]. Various equipment and strategies have been proposed to decrease the uncertainties related to the aforementioned effective parameters on masonry structures and facilitate the assessment and damage detection process [1].

A geometrical survey is a crucial part of the methodology to develop digital twins of historic structures. Nowadays, 3D laser scanners have gained attention in the structural engineering community, and engineers are trying to find optimum solutions for obtaining 3D models based on point clouds [6,7]. Various methods have been developed to automatically and semi-automatically convert the point clouds to 3D finite element models (FEMs) [8–12]. Obtaining 3D models in computer-aided (CAD) software

* Corresponding author.

https://doi.org/10.1016/j.cscm.2022.e00957
Received 25 August 2021; Received in revised form 11 February 2022; Accepted 15 February 2022
Available online 16 February 2022

packages based on the point clouds and converting the 3D model to the 3D FEMs with meshing is a conventional method that is widely used nowadays [6,13,14].

Soil-structure interaction (SSI) influences the dynamic characteristics of structures that should be considered to provide more robust simulation models [15,16]. Considering fixed-based boundary conditions is widely used for analysis and design purposes when geotechnical data is not provided [17]. But solutions for considering the SSI effects can be classified into direct and substructure approaches [15,18]. In the direct method that is considered as the most accurate modeling approach, soil, foundation, and structure are modeled by applying proper boundary conditions [18]. Studies on historical masonry structures using the direct method show the significant effects of SSI on their dynamic characteristics and seismic behavior [17,19–22]. In the substructure approach, the SSI is simulated using springs and dashpots [18]. Although the substructure approach is efficient in terms of computational efforts and is widely used in analyzing compared to the direct method [23], its accuracy has been questioned recently in [24].

Material properties are other effective parameters on the dynamic characteristics of the structures. Destructive tests on historical structures are usually forbidden due to their values, and non-destructive tests should be utilized [2,14]. Operational modal analysis (OMA) of historical masonry towers or minarets based on ambient vibrating testing (AVT) method using accelerometers has gained so much attraction recently [25–32]. Calibration of structures based on the OMA results is one of the non-destructive methods to define the material properties of historical structures and minimize the differences of the dynamic characteristics of numerical model and structure [3,33–39]. Although SSI is significantly effective on the dynamic characteristics of structures, a few studies have been done to calibrate the numerical models considering the SSI effects using the substructure method [40–44]. However, there is still a gap in the numerical model updating of historical structures so that soil parameters are also updated. Moreover, different types of SSI modeling approaches are needed to be considered, including the direct method.

Calibrated digital twins can be utilized for predicting the vulnerability of structures subjected to various types of risks, including earthquake [33,41,45–48]. Masonry structures are susceptible to seismic actions, and seismic risk assessment of historic masonry structures is a pivotal task for the authorities [49,50]. Furthermore, experiences of past earthquake events show considerable damage due to the resonance effect [51,52]. A building will approach a state of partial resonance when the fundamental period of soil and structure have matched each other, and seismic waves will be amplified that result in the increasing of inertial faces acting on the structures [53,54]. Therefore, investigating the risk of this phenomenon on existing structures and considering it for designing buildings should be taken into account even in low seismicity zones.

In this paper, a framework for developing simulation-based digital twins of historical structures using 3D laser scanners and accelerometers considering the SSI effects is explained. A digital twin of the Slottsfjell tower in the city of Tønsberg in Norway has been developed. 3D laser scanners are utilized to facilitate the geometrical survey and the procedure of the conversion of the point clouds to the FEM has been discussed. Afterward, AVT was done, and three frequency domain OMA methods were utilized to derive the tower's natural frequencies and mode shapes. SSI effects are considered using both the direct (DM) and substructure (SM) methods, and a model with fixed-based (FB) boundary conditions has been developed without considering the SSI effects. The tower was constructed by the tønsbergite stone, and mechanical properties of the stone were utilized to derive the base values of the material properties of the homogenized masonry for performing sensitivity analysis and the FEM updating. A sensitivity analysis is performed to investigate the most effective parameters on the dynamic characteristics of the tower for the three mentioned FEMs and the results are compared to each other. FEM updating of the three models was done by updating the SSI parameters, and the results of the updated materials have

Fig. 1. (a) Location of Tønsberg in Norway, (b) Different views of the Slottsfjell tower, and (c) Geometry of the tower.

been compared to each other. After providing the calibrated DM model, the risk of resonance effect has been evaluated. Finally, linear time history has been carried out on all three calibrated models and the results are compared to each other.

2. Overview of the case study

The Slottsfjell tower is in the city of Tønsberg in the southeastern part of Norway (see Fig. 1(a)). It is centrally located in the ruined park from one of the Nordic region's largest medieval castles. The tower is not older than 150 years and was built to celebrate 1000 years since the city of Tønsberg was founded in 871. On top of the entrance, it is written the years 871–1871 with the corresponding text "May the city that stands on the hill, flourish a thousand new year" in Norwegian. Fig. 1(b) shows the Slottsfjell tower in different views. The tower is made of stone masonry with a square shape which can typically be seen in medieval constructions. The tower has a historical value for the county of Vestfold and Telemark because of the region's identification with the Viking age due to the most magnificent burial site from the Viking era in Norway located in that area. The tower's total height is 21 m, with one basement and three stories on top of the soil level. Each story is like a box, and the width of each box is decreased from the basement level to the top floor. The geometry of the tower is depicted in Fig. 1(c).

3. Numerical modeling

3.1. 3D Geometric documentation

Totally twenty scans were performed using a Topcon 2000 3D laser scanner inside and outside the tower to provide dense point clouds. The raw point clouds of the scans were imported to Autodesk Recap Pro software [55] to be combined, and a unique dense point cloud model is provided as depicted in Fig. 2(a), and each circle shows the location of the scans. The 3D point cloud file is imported to Autodesk Revit software [56], as illustrated in Fig. 2(b). The 3D model of the tower was provided in the Revit software based on the point clouds as presented in Fig. 2(c).

3.2. Finite element modeling

A semi-automatic procedure to provide the 3D FEM based on the point clouds data was utilized in this study. After providing the 3D model of the tower, the industry foundation classes (IFC) format of the model was exported from the Revit Autodesk software. The CAD exchanger software was utilized to convert the IFC format file to the standard for the exchange of product model data (STEP) format, which is suitable for importing the 3D solid models in DIANA FEA [57] software to develop the 3D FEM. After importing the STEP file to DIANA FEA, several cleaning tools have been chosen to modify the 3D model, including healing the edge inaccuracies, removing duplicate surfaces and small entities, etc.

For 3D finite element modeling of the tower, the homogenized method has been considered by neglecting the discretization of masonry units and mortar, which is widely used for modeling full-scale structures [58,59]. This approach needs fewer input data and less computational effort than the discrete element method which masonry units and mortar are modeled separately by defining the interface elements [4].

Fig. 2. (a) Point clouds derived from the 3D laser scanner and position of the scanners during the data acquisition, (b) imported dense 3D point to the Revit Autodesk software, and (c) 3D drawing of the tower in the Revit Autodesk software.

3.3. Soil-structure interaction modeling

Three models with three various boundary conditions were developed. For the FB model, the SSI was neglected by employing rigid supports in three degrees of freedom beneath the tower, as illustrated in Fig. 3(a). Note that neither soil spring nor rigid supports are not modeled around the basement walls, based on [60].

The second model (SM) is provided based on the substructure method to consider the SSI by modeling springs beneath the tower, as depicted in Fig. 3(b). Based on the Winkler method, springs have stiffness in three directions to support the normal and shear stiffnesses [61].

The third model (DM) is characterized by modeling the foundation and soil box as the most detailed model in terms of considering the SSI effects (see Fig. 3(c)). In this model, the foundation is modeled beneath the tower as a box with a height of 2.5 m based on the data provided by the slottsfjell museum. Regarding the dimension of the soil box, the depth and the length should be considered larger than 1,5 and 3 times the dimension of the foundation based on [62]. Therefore, the soil box is modeled with the depth and length of 11 m and 22 m, respectively. Rigid boundary conditions are considered for the bottom of the soil box, but for four side faces of the box, roller supports are employed to constrain the displacement in the normal direction of the faces [15,63].

The FEMs are developed in the DIANA FEA software and then imported to the FEMtools software [64] for performing future analyses. Hexahedron mesh type was chosen for meshing the model, so that hexahedron elements are the dominant choice, and tetrahedron and pentahedron mesh elements were used to fill parts of the geometry. The total number of elements of the FB, SM, and DM models are 66,676, 66,286, and 93,832, respectively, with a maximum mesh size of 65 cm.

3.4. Material properties of soil and masonry

The Slottsfjell tower was constructed using the tønsbergite stone, which is a variant of the Norwegian igneous rock larvikite and the

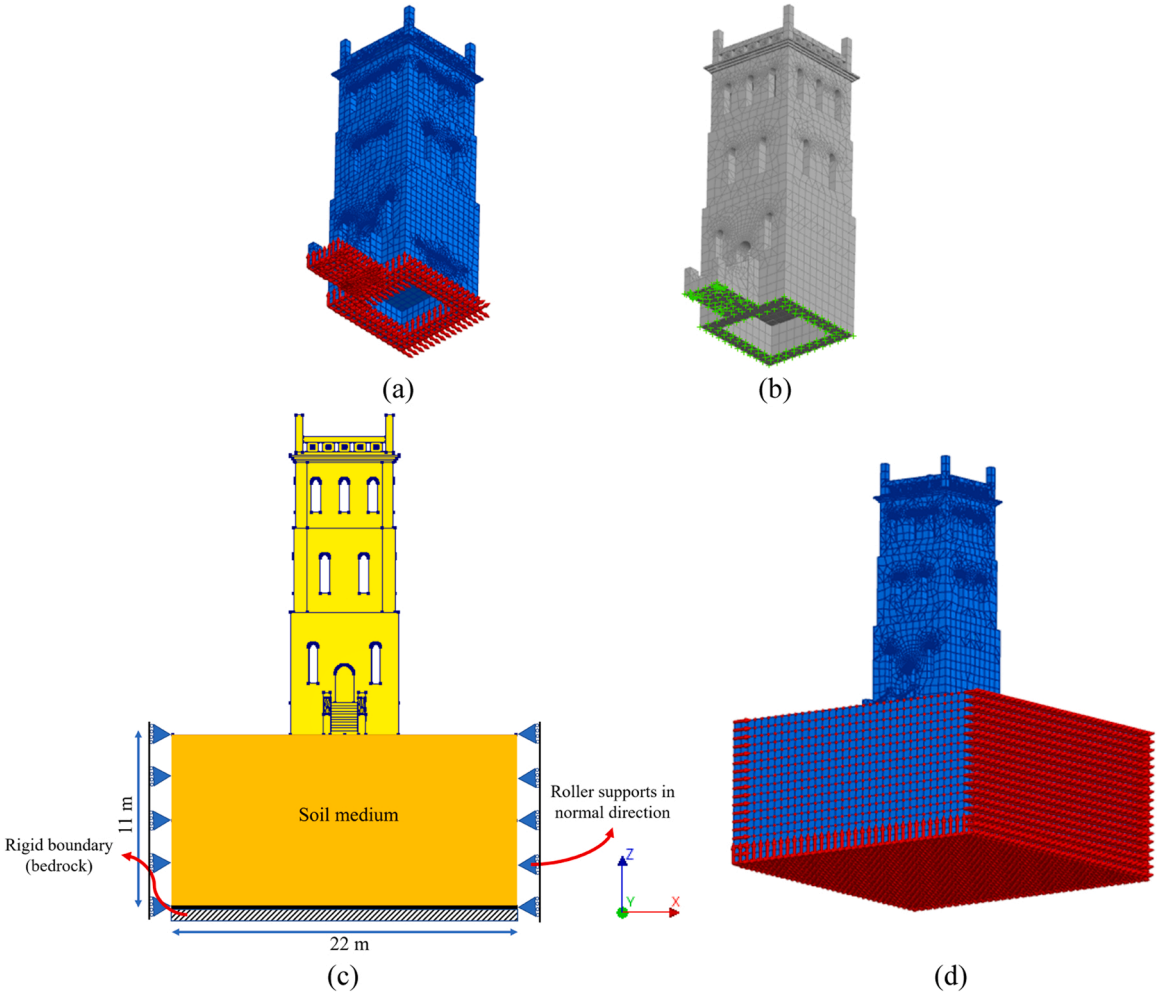

Fig. 3. The 3D mesh of (a) FB, (b) SM models, (c) detail of modeling DM model, and (d) 3D mesh of DM model of the tower.

larvikite rock is classified as a variant of the monzonite rock [65,66]. Compared to granite, which is more broadly known, monzonite has a lower percentage of quartz [67]. The elasticity modulus of the stone unit is considered 61 GPa based on [68], and stiff mortar type is considered with an elasticity modulus value of 12 GPa based on [69]. Orthotropic material is considered for masonry, and homogenized masonry properties are derived based on an empirical equation presented in [70]. Although the elasticity modules of the homogenized masonry derived from the empirical equations are more than the real values since the deformations of the bed joint mortar are not considered [70], the value can be utilized for the base value and will be updated through the calibration process. Furthermore, the shear modulus of masonry is considered 0.15 times the elasticity modulus based on [36,71].

Since no laboratory test has been conducted on the soil properties, hard soil properties based on the field investigation and the properties are selected based on [15]. Normal subgrade reaction factor of the boundary condition of the SM is calculated based on the simplified Vesic model [72] and Eq. (1).

$$K_z = \frac{E_s}{B.(1-\nu_s{}^2)} \tag{1}$$

Where E_s and ν_s are the elasticity modulus, and the Poisson's ratio of soil, respectively, and B is the foundation length. Furthermore, the shear stiffnesses (K_x and K_y) are considered 0.01 times of the normal stiffness [73,74]. All material properties and spring reaction factors are summarized in Table 1, which are utilized for the sensitivity analysis and the base values for the model updating in the next sections. It should be noted that as a limitation of this model, the effect of foundation interaction is neglected. Moreover, the springs have the same stiffness in different locations beneath the tower, which is not realistic considering the non-homogeneous behavior of soil and foundation. Orthotropic material was considered for the soil media of the DM model with mechanical properties of the hard soil [15] as presented in Table 1.

4. Sensitivity analysis on the effects of material properties

To have a better understanding of the effective parameters on the dynamic characteristics of the tower, a sensitivity analysis was done. The tower is discretized into different sets, as illustrated in Fig. 4. The same set names based on the order of the sections that appeared in Fig. 4 for the first floor (sets 2–6) were considered for the sets of the second and the third floor. For the DM model, the soil and foundation are discretized into eight and four sections, respectively. The soil box is halved in all dimensions to be discretized to eight sets, and the foundation is divided into four equal sets in plan view. Elasticity modulus and shear modulus of different sets of masonry in three directions are considered the parameters. Their influence is investigated on the first five natural frequency values of the three developed models of the tower.

Fig. 5 depicts the sensitivity graphs of the elasticity modulus for the three developed models. It can be concluded that Ez is the most effective parameter that mostly influences the first two natural frequencies. Moreover, higher sensitivities are related to the first-floor elements compared to other floors. The graphs also show that the changes in elasticity modulus of the foundation and soil sets have less effect on the frequencies than the masonry material properties.

Based on the sensitivity graph of the shear modulus presented in Fig. 6, G_{xy} is the least effective parameter, and responses are more sensitive to G_{yz} and G_{xz}. Sensitivity values are highest for the first-floor sets and lowest for the third-floor sets. Unlike the elasticity modulus, it should be noted that the shear modulus is effective on higher modes. The graphs also show that the changes in shear modulus of the foundation and soil sets have negligible effects on the frequencies compared to the masonry material properties.

A sensitivity analysis is performed to investigate the effect of spring stiffnesses of the SM model's boundary conditions, and the graph is illustrated in Fig. 7. K_z is the most effective parameter that affects more on the first two modes' frequencies, and the torsional mode is highly sensitive to K_x. By comparing the normalized sensitivity values of the sensitivity graph illustrated in Fig. 7, with other parameters' sensitivity values presented in previous graphs, it can be pointed out that the SM model is more sensitive to springs' stiffnesses values than the masonry properties.

Table 1
Material properties of the homogenized stone masonry of the tower, soil, normal and shear reaction factors of boundary conditions of the SM model.

Material	Properties	Value
Masonry	Density (kg/m^3)	2800
	Elasticity modulus in X, Y and Z directions (E_x,E_y,E_z) (GPa)	40
	Shear modulus in XY, YZ and ZY directions (G_{xy},G_{yz},G_{zy}) (GPa)	6
	Poisson ratio in XY, YZ and ZY directions (u_{xy}, u_{yz}, u_{zy})	0.25
Soil	Density (kg/m^3)	2000
	E_x,E_y,E_z (GPa)	6
	G_{xy},G_{yz},G_{zy} (GPa)	0.9
	u_{xy}, u_{yz}, u_{zy}	0.3
Spring	Normal reaction factor (K_z) (GPa/m)	51.2
	Shear reaction factor (K_x,K_y) (GPa/m)	0.512

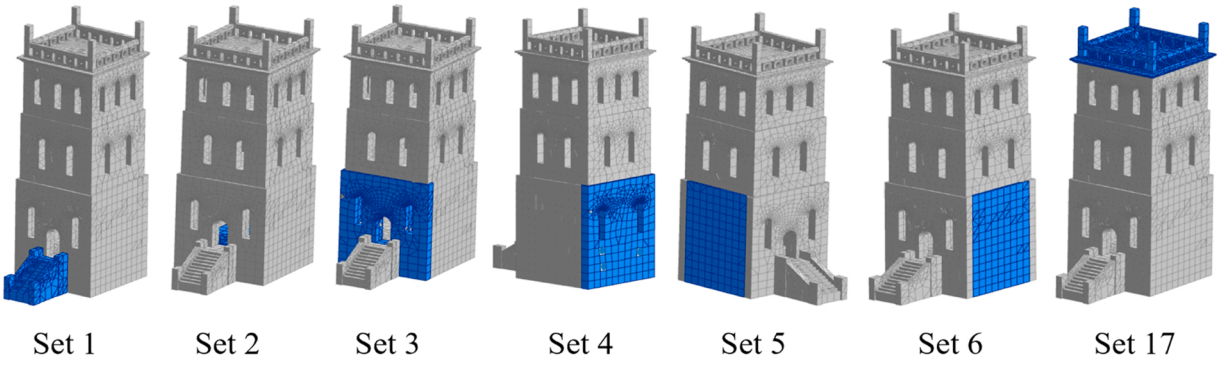

Fig. 4. The different sets of the tower and their corresponding names.

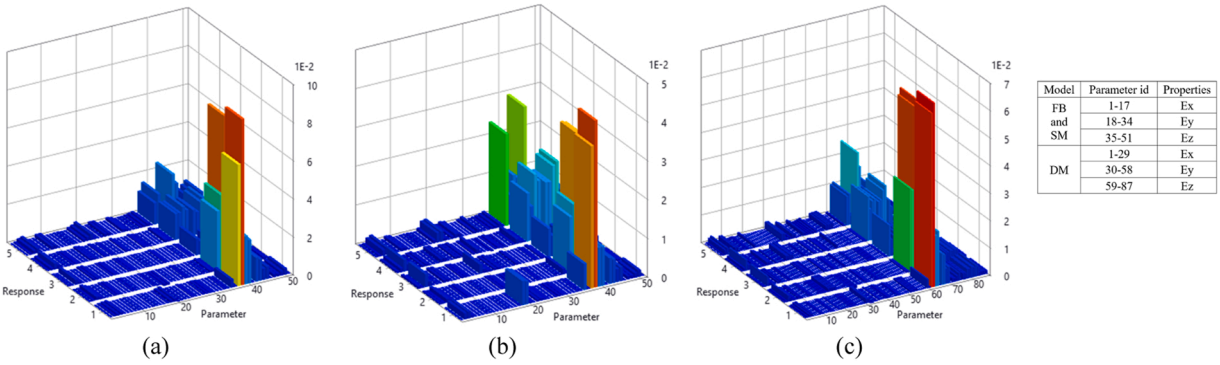

Model	Parameter id	Properties
FB and SM	1-17	Ex
	18-34	Ey
	35-51	Ez
DM	1-29	Ex
	30-58	Ey
	59-87	Ez

Fig. 5. Sensitivity graphs to a change in elasticity modulus for the (a) FB, (b) SM, and (c) DM models.

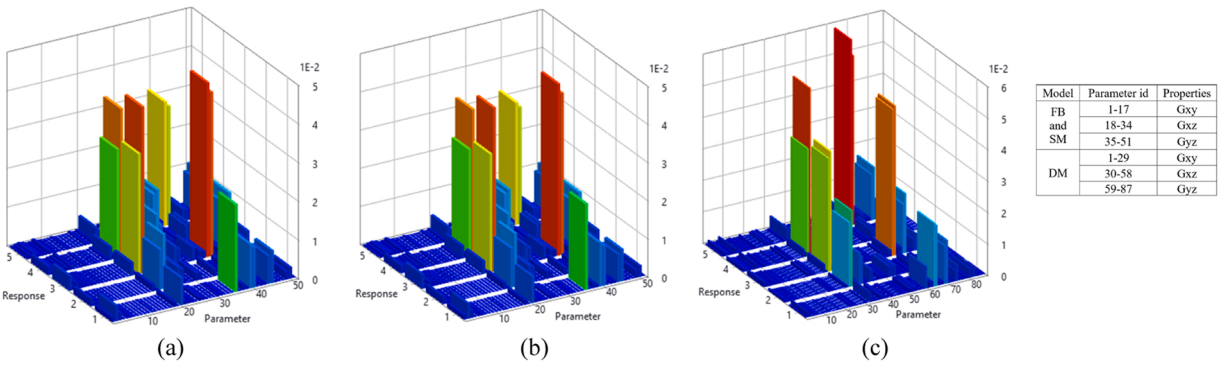

Model	Parameter id	Properties
FB and SM	1-17	Gxy
	18-34	Gxz
	35-51	Gyz
DM	1-29	Gxy
	30-58	Gxz
	59-87	Gyz

Fig. 6. Sensitivity graphs to a change in shear modulus for the (a) FB, (b) SM, and c) DM models.

5. System identification

5.1. Ambient vibration testing

Ambient vibration testing was performed using 3-Axis MEMS digital Unquake accelerometers with a sampling rate of 250 Hz. Compared to the more sensitive piezoelectric accelerometers, lower cost and power consumption are two main characteristics of MEMS accelerometers [1,47]. However, the reliability of the OMA results of various low-cost MEMS accelerometers was confirmed with low error values compared to the low-noise piezoelectric accelerometers [75].

The accelerometers' locations have been decided based on engineering judgment and previous studies [3,36], as depicted in Fig. 8 (a). The accelerometers are equipped with the global positioning system (GPS) antenna and a global navigation satellite system (GNSS) receiver. GPS data were used to record the time and synchronize all the data from the accelerometers based on the recorded time. Fig. 8 (b) shows the test setup, and Fig. 8(c) shows a sample of an acceleration graph derived from an accelerometer.

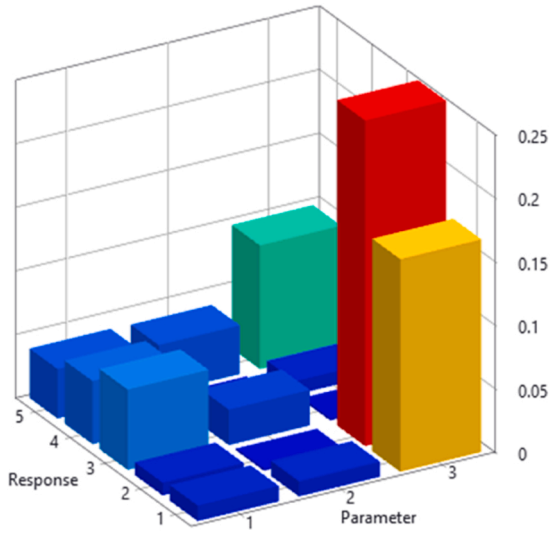

Model	Parameter id	Properties
SM	1	Kx
	2	Ky
	3	Kz

Fig. 7. Sensitivity graph to a change in spring stiffnesses of the SM model.

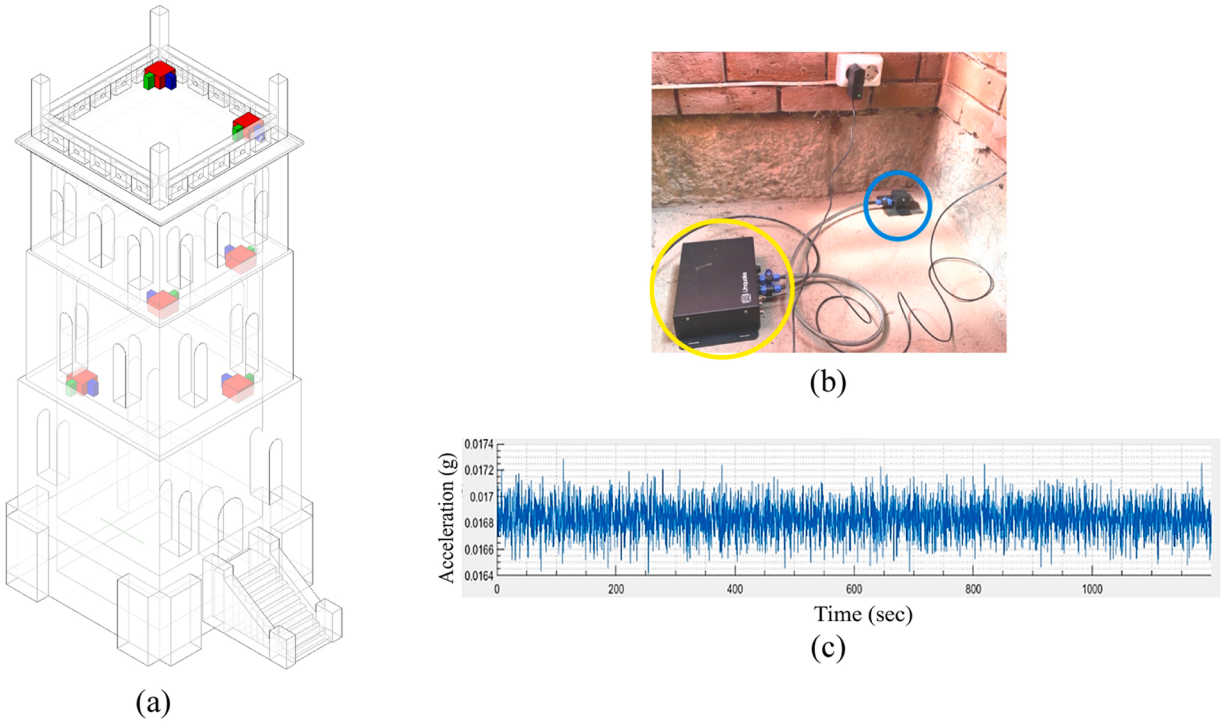

Fig. 8. (a) Locations of the accelerometers [66], (b) test setup including the accelerometer (in blue circle) and datalogger (in yellow circle), and (c) sample of an acceleration graph derived from an accelerometer.

5.2. Operational modal analysis

A preliminary analysis has been done by performing Fast Fourier Transform (FFT) on single sensor measurements in [76]. For confirming the results, frequency domain methods are utilized to investigate the dynamic characteristics of the tower based on the distributed sensor network measurements. Frequency Domain Decomposition (FDD), Enhanced Frequency Domain Decomposition (EFDD), and Curve-Fitted Enhanced Frequency Domain Decomposition (CFDD) methods are three frequency-domain methods that were utilized to derive the natural frequencies and corresponding mode shapes of the tower. The idea of FDD method is to carry out an approximate decomposition of a system response into a set of independent single-degree-of-freedom systems for each mode. First, the

spectral density matrices are estimated. Singular value decomposition of the spectral density matrices is done, and finally, the peak pick on the average singular values will be performed to derive the modal parameters [77,78]. EFDD and CFDD are the improved versions of the FDD method that damping ratio estimation is available, and the accuracy of the dynamic characteristics is enhanced. In EFDD, the FDD peak picking is extended with a simple time domain least squares estimation technique, and in CFDD, the extension relies on a frequency domain least squares estimation technique [79,80]. Artemis Modal software was utilized to perform the operational modal analysis [81]. The differences between the values of the natural frequencies are negligible (less than 0.3%); moreover, the mode shapes are equal. Therefore, the singular value decomposition (SVD) graph of the FDD method is reported in Fig. 9(a), and the five first peaks of the graph were selected to represent the first five modes of the tower. Mode shapes and corresponding frequency values of the first five modes of the tower are illustrated in Fig. 9(b). All modes are flexural except the third mode, which is a torsional mode.

6. Finite element model updating

After performing sensitivity analysis to understand the effect of material properties on the dynamic characteristics of the tower and performing system identification to derive the first five natural frequencies and mode shapes of the real structure, the FEM updating is the last step to develop the digital twins.

The objective of model updating is to adjust the selected parameters' values so that a reference correlation coefficient is minimized. The weighted absolute relative difference between resonance frequencies and the weighted difference between target and average actual modal assurance criteria (MAC) are two correlation coefficients that are considered through the FEM updating procedure. MAC value is a measure of the squared cosine of the angle between two modes shapes that is derived based on Eq. (2).

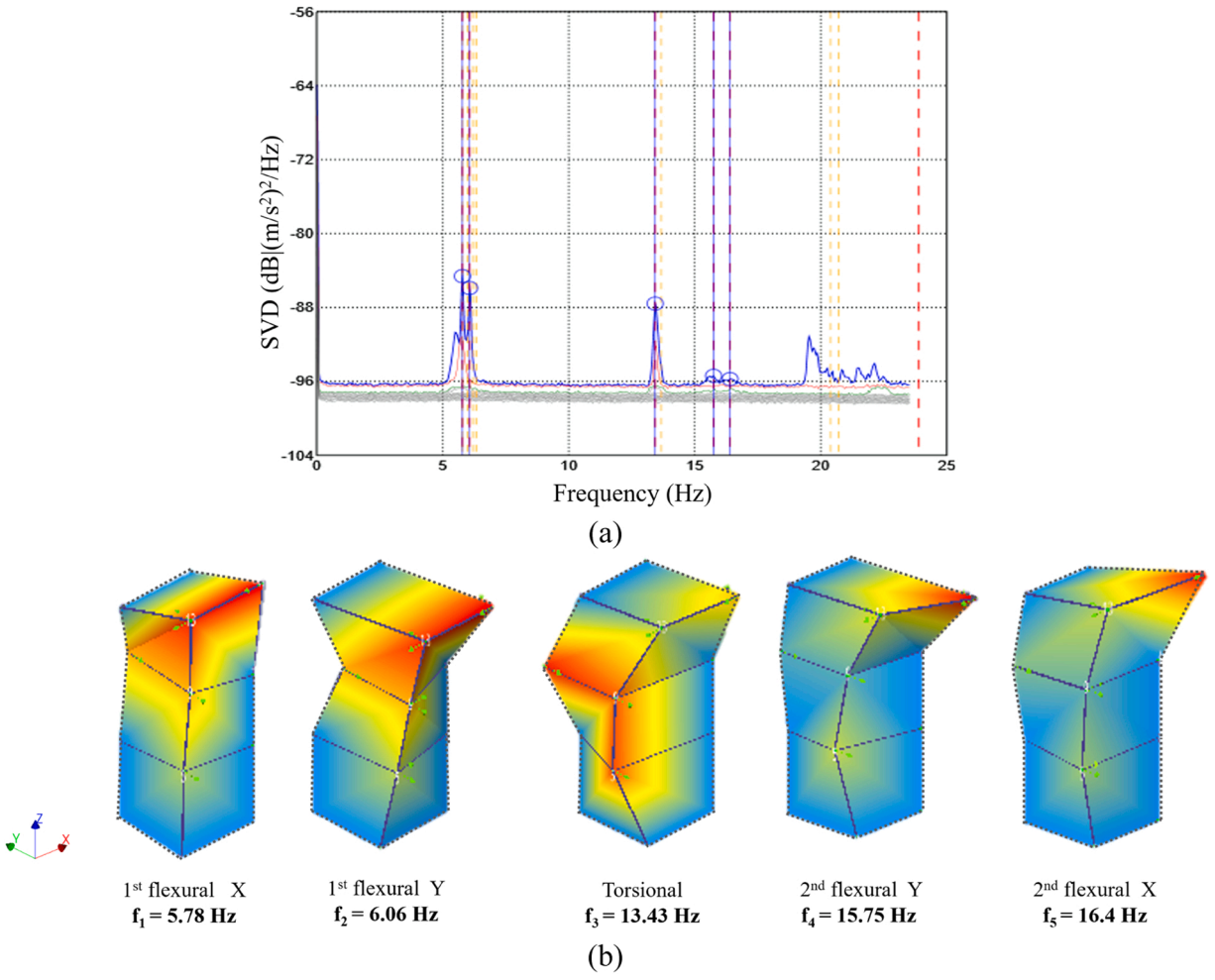

Fig. 9. (a) SVD graph of the FDD method, and (b) mode shapes and corresponding frequencies of the tower based on the OMA results.

$$MAC(\psi_a, \psi_e) = \frac{\left|(\{\psi_a\}^t\{\psi_e\})\right|^2}{(\{\psi_a\}^t\{\psi_a\})(\{\psi_e\}^t\{\psi_e\})} \quad (2)$$

Where ψ_e and ψ_a are respectively the experimental and analytical eigenvectors. Bayesian parameter estimation by minimizing a weighted error as presented in Eq. (3) is utilized for FEM updating in the FEMtools software package.

$$E = \{\Delta R\}^t[C_R]\{\Delta R\} + \{\Delta P\}^t[C_P]\{\Delta P\} \quad (3)$$

Where ΔR is a difference between a vector containing the reference and predicted system responses, ΔP is a difference between a vector containing the given state and predicted system parameters, C_R and C_P represent weighting matrices expressing the confidence in the model responses and parameters respectively.

FEM updating was done on the FB model, and absolute differences of frequency values (ADFV) derived from the OMA and FEA are presented for the first five modes of the model in Table 2. A good correlation between the frequency values of the first two modes is reached after the updating process, but the differences for the other modes are high. Moreover, MAC values and a 3D plot are presented in Fig. 10 (a) and (b), respectively. MAC values show the same correlations for the first two modes, but the differences of the higher modes are significant. Based on the MAC value matrix in Fig. 10 (a), modes 4 and 5 of FEA are paired to modes 5 and 4, respectively. However, since the modes are not in sequence based on the frequency values, this correlation is not accepted, and diagonal MAC values should be considered for the pairing modes. Fig. 10 (c) shows the paired mode shapes of the first three modes to show the correlation between the mode shapes derived from the FEA and the OMA after model updating.

FEM updating of the SM model was performed by calibrating the masonry and the boundary condition spring stiffnesses. Based on Table 3, frequency values of the first three modes are close enough, but ADFVs more than 5% can be seen for the other modes. Moreover, all mode shapes are paired with MAC values of more than 65% based on Fig. 11.

FEM updating of the DM model was done by calibrating the masonry, foundation, and soil material properties. Based on Table 4, differences between the frequencies' values are negligible, with values less than 3%. Moreover, based on Fig. 12 (a) and (b), MAC values of more than 65% depicts that mode shapes from FEA follow the OMA mode shapes, and lower values for the off-diagonal MAC matrix show a good correlation of the modes shapes and Fig. 12 (c) also approves the good correlation of the mode shapes.

6.1. Comparison of updating results

To compare the calibration results for the three FEMs, the average values of ADFVs are presented in Fig. 13 (a). Moreover, MAC values of the first five modes (corners of the diagram) are depicted in Fig. 13 (b) for the three developed and updated FEMs. Based on Fig. 13 (a), The average ADFVs are decreased by considering the SSI effect in the numerical models, and the DM model is considered as the most robust model with an average ADFV of 1.6%.

This claim is also approved based on Fig. 13 (b) since higher MAC values are derived from the models that SSI effects are considered. Furthermore, the DM model is considered as the closest updated model to the test in terms of the mode shapes. The MAC values of the first two modes do not change considerably for the FB and SM models, but the MAC values of the higher modes are increased in the SM model. Moreover, in the DM model compared to the SM model, MAC values of the first modes are improved, but no significant improvement is reached for other modes.

6.2. Comparison of updated material properties

In order to compare the material properties of the updated models, E_z is the most effective parameter on the first two natural frequencies, G_{xz} and G_{yz} are effective parameters on higher modes that are chosen based on the performed sensitivity analysis. Fig. 14 shows the average values of the parameters for each floor that is presented for the three models. The changes in material properties in different floors for the FB model are not as significant as the other two models. Furthermore, based on Fig. 14 (a), in both models with SSI effects, E_z of the second floor has a lower value compared to the other two floors. Based on Fig. 14 (b) and (c), the shear modulus of the second floor is more than two other floors in the DM model, but it is not reported in two other models. Except for the E_z of the second floor and the SM model, other updated material properties for the models with SSI effects are more than the FB model. Therefore, in terms of linear material properties effective on the structural stiffness, calibrated results of the FB model are conservative with lower values.

Updated values for the spring stiffnesses of the boundary condition of the SM model and average values of the selected material

Table 2
OMA and FEA natural frequencies and ADFVs for the first five modes of the FB model.

Modes	OMA frequencies (f_e)	FEA frequencies (f_a)	ADFV (%)
1	5.778	5.757	0.365
2	6.063	6.009	0.899
3	13.428	10.964	22.473
4	15.747	17.513	10.084
5	16.398	18.165	9.727

FEA modes \ OMA modes	1	2	3	4	5
1	64.9	15.3	1.3	0.7	15.9
2	34.8	84	0.6	20.3	0.2
3	5.2	14.2	56.1	11.6	23.5
4	0.8	0.2	2.6	1	61
5	0.5	2.6	3.3	70.5	0.8

(a)

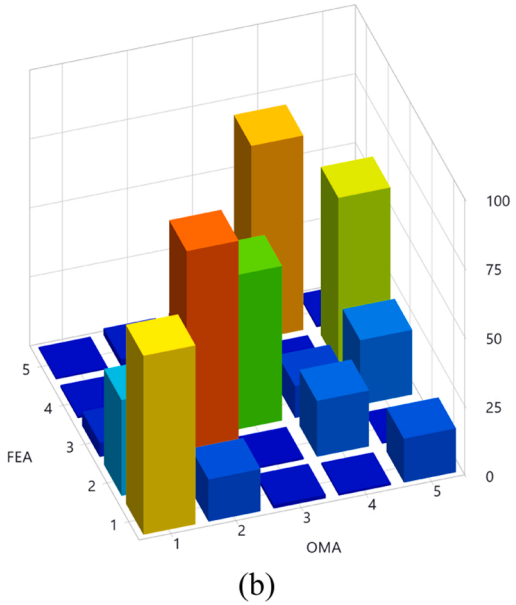

(b)

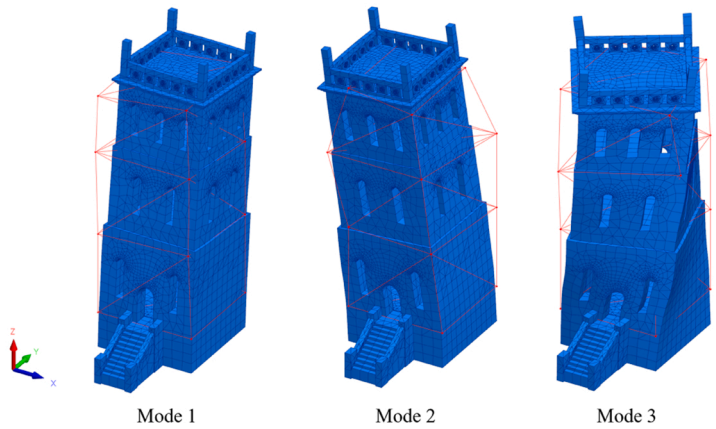

(c)

Fig. 10. (a) MAC matrix, (b) 3D MAC plot, and (c) mode shape pairing of the first three modes of the FB model after model updating.

Table 3
OMA and FEA natural frequencies and ADFVs for the first five modes of the SM model.

Modes	OMA frequencies (f_e)	FEA frequencies (f_a)	ADFV (%)
1	5.778	6.065	4.963
2	6.063	6.11	0.774
3	13.428	13.661	1.738
4	15.747	16.816	6.789
5	16.398	17.61	7.398

properties of the soil and foundation are presented in Table 5. The normal reaction factor of the soil-foundation is increased, but the shear values for all to directions are decreased after the calibration process in the SM model. For the DM model, no significant change can be seen for the foundation and soil compared to the changes of the spring stiffnesses in the SM model.

7. Resonance effect and dynamic analysis

In this section, firstly, the resonance effect has been evaluated for the tower based on the calibrated DM model. Moreover, a code equation has confirmed the results from the modal analysis of the soil media in the DM model. Afterward, time history analysis was performed on the three calibrated models by applying two seismic records, and the results were compared.

FEA modes \ OMA modes	1	2	3	4	5
1	65.9	14.8	8.1	1.2	15.9
2	34	84.5	0.2	19	0.3
3	3.2	14.6	66.7	7.8	17.4
4	6.8	13.9	5.6	80.8	0.9
5	8.9	4.4	7.6	7.2	73.3

(a)

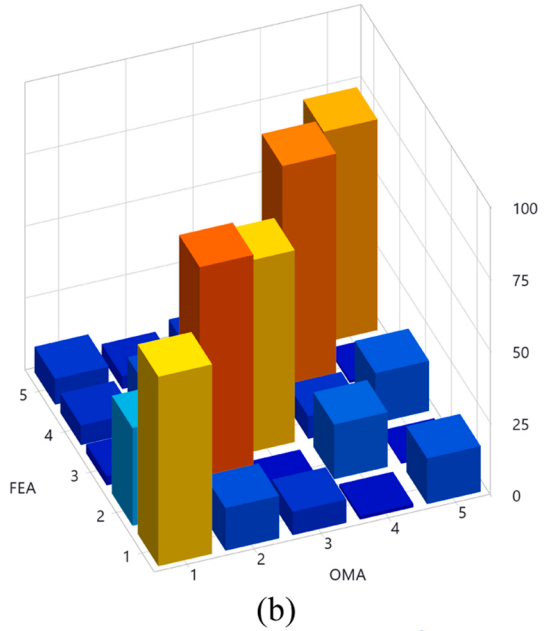

(b)

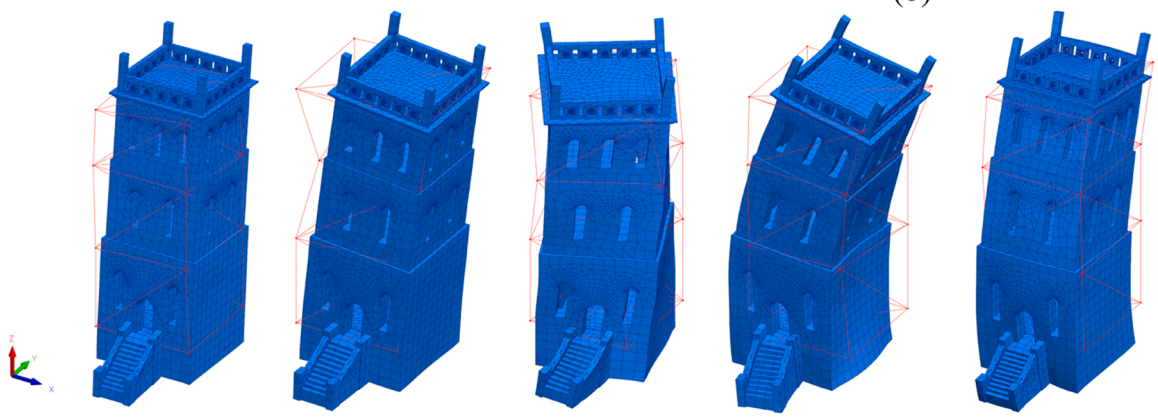

(c)

Fig. 11. (a) MAC matrix, (b) 3D MAC plot, and (c) mode shape pairing of the first five modes of the SM model after model updating.

Table 4
OMA and FEA natural frequencies and ADFVs for the first five modes of the DM model.

Modes	OMA frequencies (f_e)	FEA frequencies (f_a)	ADFV (%)
1	5.778	5.838	1.05
2	6.063	6.123	0.99
3	13.428	13.53	0.76
4	15.747	16.22	3
5	16.398	16.773	2.29

7.1. Resonance effect

The fundamental period of the soil box of the calibrated DM model is 0.044 s based on the modal analysis. In order to confirm the result of the modal analysis of the FEM, the fundamental period of the soil box was calculated using Eq. (4) presented by SHAKE code [82].

$$T = \frac{4SLT}{(2n-1)V_s} \tag{4}$$

		OMA modes				
		1	2	3	4	5
FEA modes	1	99.4	3.3	0.8	13.6	15.5
	2	0	95.1	5.5	9.4	4.7
	3	4.1	14.1	66.1	8	18.7
	4	4.3	3.3	4.4	85.2	2.5
	5	11.7	6.4	9.6	6.4	77.3

(a)

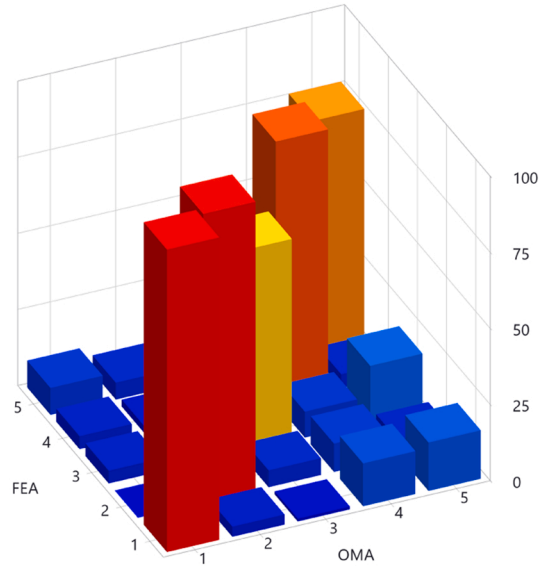

(b)

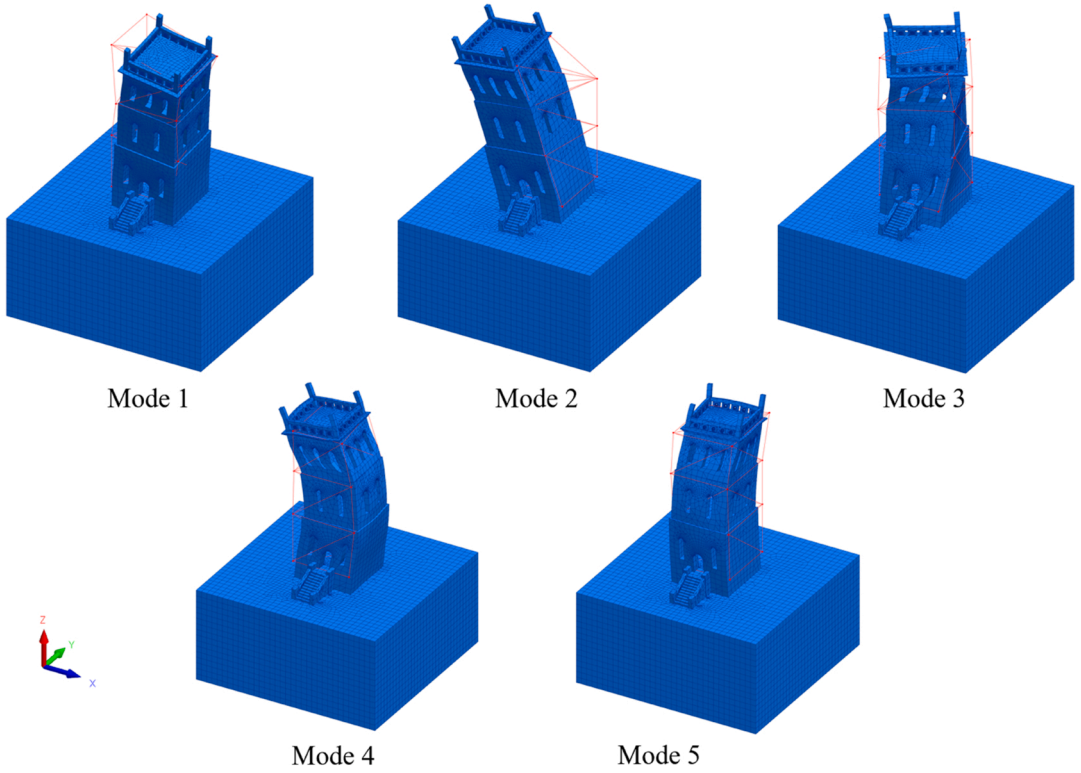

(c)

Fig. 12. (a) MAC matrix, (b) 3D MAC plot, and (c) mode shape pairing of the first five modes of the DM model after model updating.

Where T is the fundamental period of soil, SLT is the soil layer thickness above the bedrock, n is the mode number and V_s is the soil shear wave velocity.

Considering 11 m for SLT based on the model assumption, and 1000 $\frac{m}{s}$ for the V_s as suggested in [21], for hard soil, 0.044 s is calculated as the fundamental period ($n = 1$) and confirms the results from the finite element analysis. However, natural period of the tower is more than three times the fundamental period of soil. Therefore, the resonance effect cannot influence the tower structural

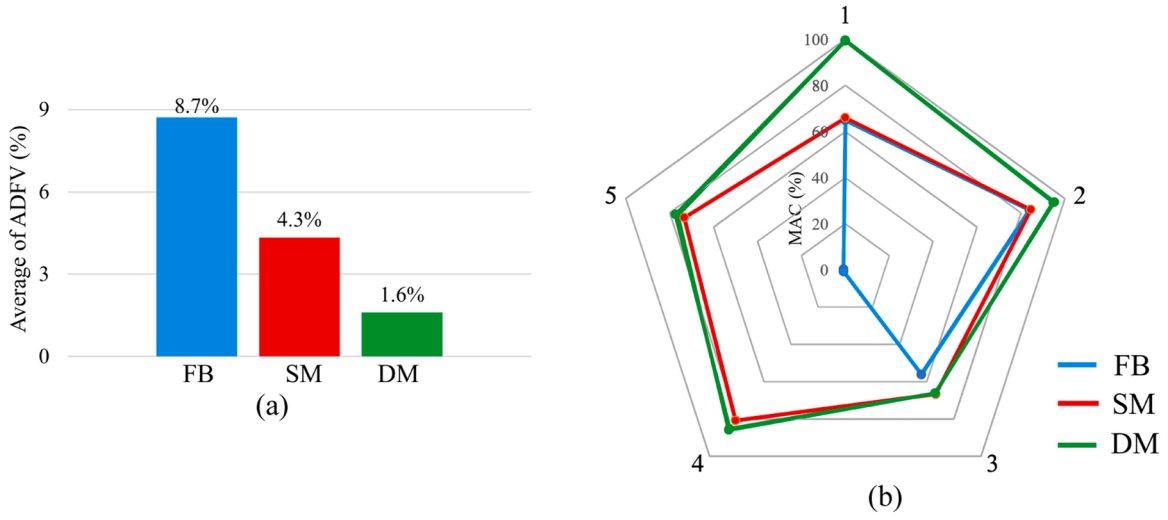

Fig. 13. (a) Average values of the ADFVs, and (b) MAC values for the first five modes of the three developed models.

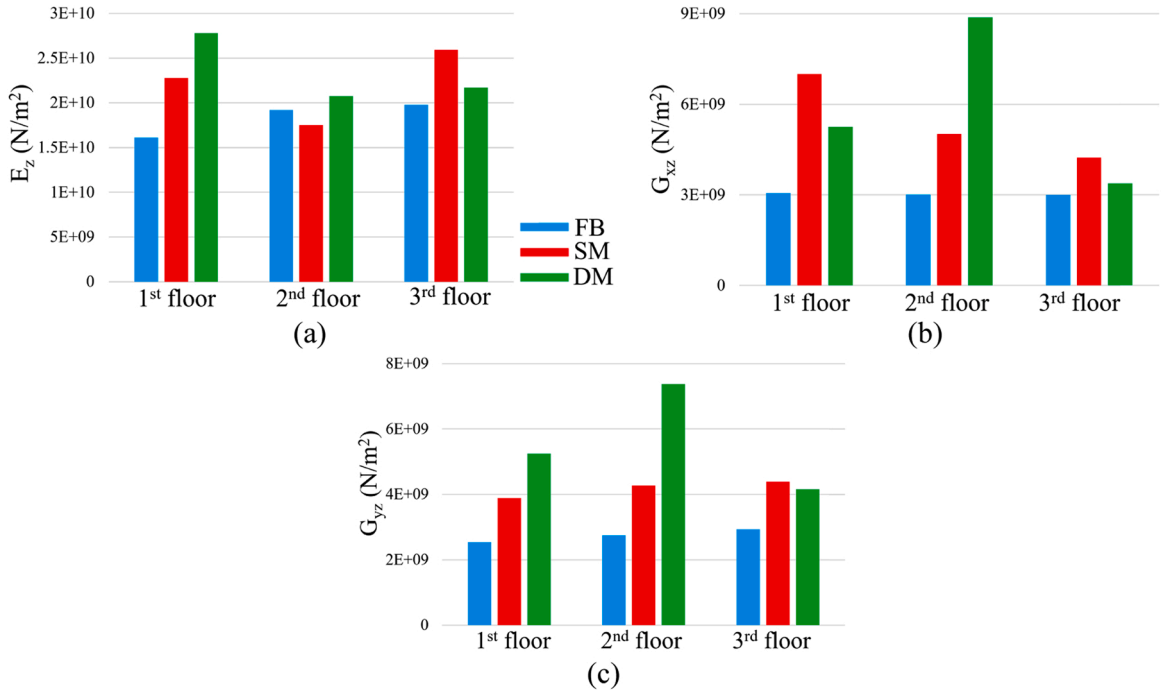

Fig. 14. Updated values of the three developed FEMs presented for three floors: (a) E_z, (b) G_{xz}, and (c) G_{yz}.

behavior subjected to vibrations.

7.2. Time history analysis

Tønsberg is located in a low seismicity zone with peak ground acceleration (PGA) of 0.02–0.03 g, as illustrated in the seismic hazard map [83], in Fig. 15 (a). However, in order to perform a comparative study on the structural response of the calibrated models subjected to seismic excitations, linear time history analysis was carried out by applying two far-field seismic records in the X direction. Fig. 15 (b) and (c) shows the acceleration versus time plots of Manjil and Northridge seismic records that have been chosen from the PEER strong ground motions database [84], and detail about them are provided in Table 6.

Rayleigh damping coefficients were computed considering 5% damping ratio for the first and third modes of vibration [85]. For the DM model, mass and stiffness damping coefficients of hard soil are $3.92\,\frac{1}{s}$ and $0.00047\,s$ based on [21]. The results of top

Table 5
Base and updated values of soil parameters in SM and DM models.

Model name	Parameter	Base value	Updated value
SM (GPa/m)	K_x	0.512	0.15
	K_y	0.512	0.15
	K_z	51. 2	114
DM (foundation in GPa)	E_z	40	41.1
	G_{xz}	6	5.97
	G_{yz}	6	5.61
DM (soil in GPa)	E_z	6	5.4
	G_{xz}	0.9	1.05
	G_{yz}	0.9	0.63

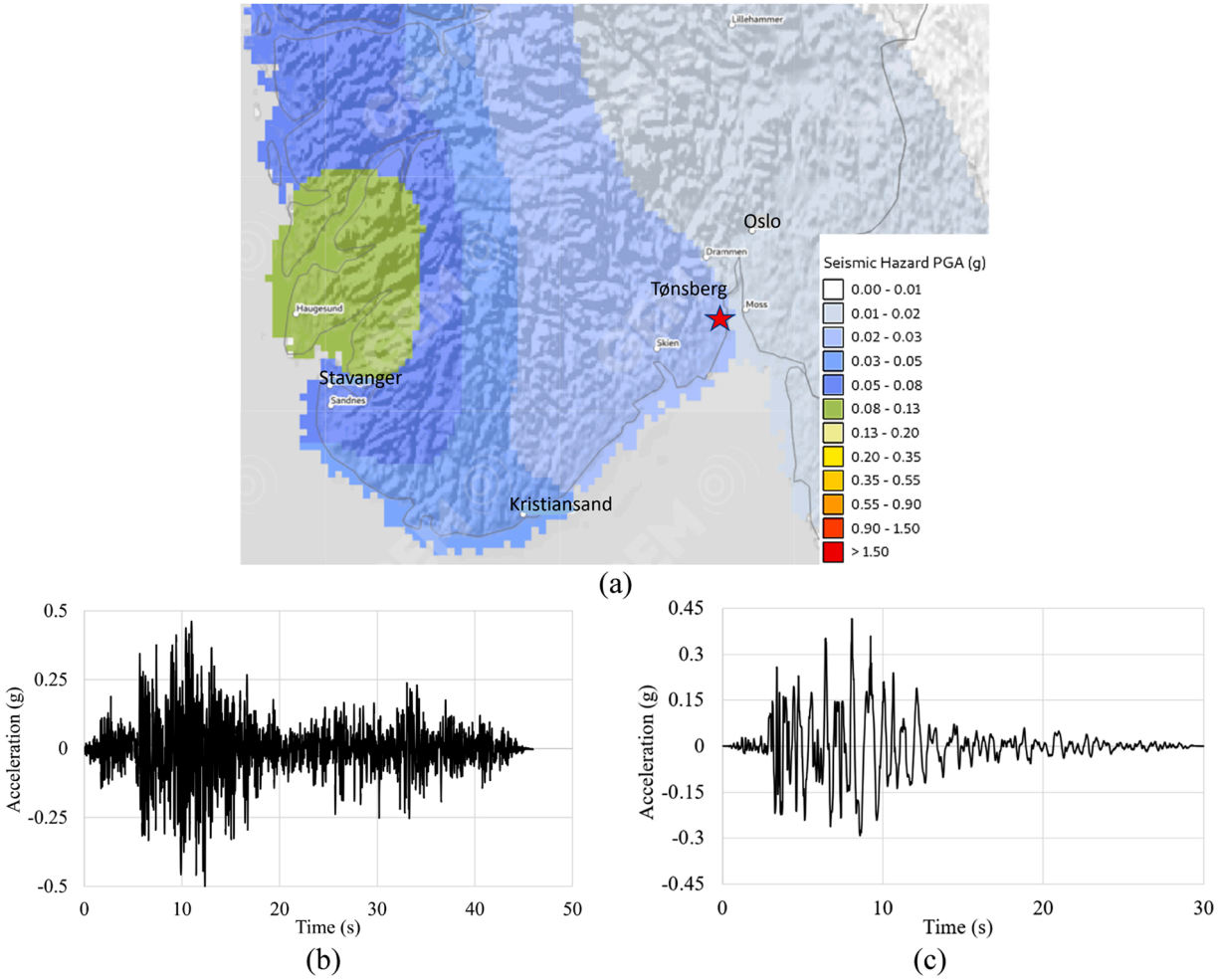

Fig. 15. (a) Seismic hazard map of southern Norway cities including Tønsberg [83], and acceleration versus time plots of (b) Manjil and (c) Northridge seismic records [84].

Table 6
Detail of the Manjil and Northridge seismic records [84].

Event	Station	Year	Magnitude	Duration (s)	Time step (s)	PGA (g)	Arias intensity ($\frac{m}{s}$)
Manjil	Abbar	1990	7.37	45.96	0.02	0.49687	7.5
Northridge	Beverly Hills	1994	6.69	29.99	0.01	0.416	4.5

displacement versus time of the three models are presented in Fig. 16 (a) and (b) for Manjil and Northridge records, respectively. Furthermore, to facilitate the comparison, maximum top displacement values of all models are presented in Fig. 16 (c) for both records. Negligible differences can be detected and differences between the maximum top displacement (less than 10%). As it is shown in Fig. 16 (c), maximum inter-story drift ratios (IDR) of the DM model subjected to both records are more than other models. Therefore, FB and SM models show more conservative results in terms of IDR, which is a parameter for defining structural safety. IDR of 0.13% is considered for light damage, which is the first limit state for stone and brick masonry buildings based on [86]. The maximum IDR values of the tower for both analyzes are less than 0.13% which can confirm the tower passed the acceptability check and did not satisfy the failure criteria.

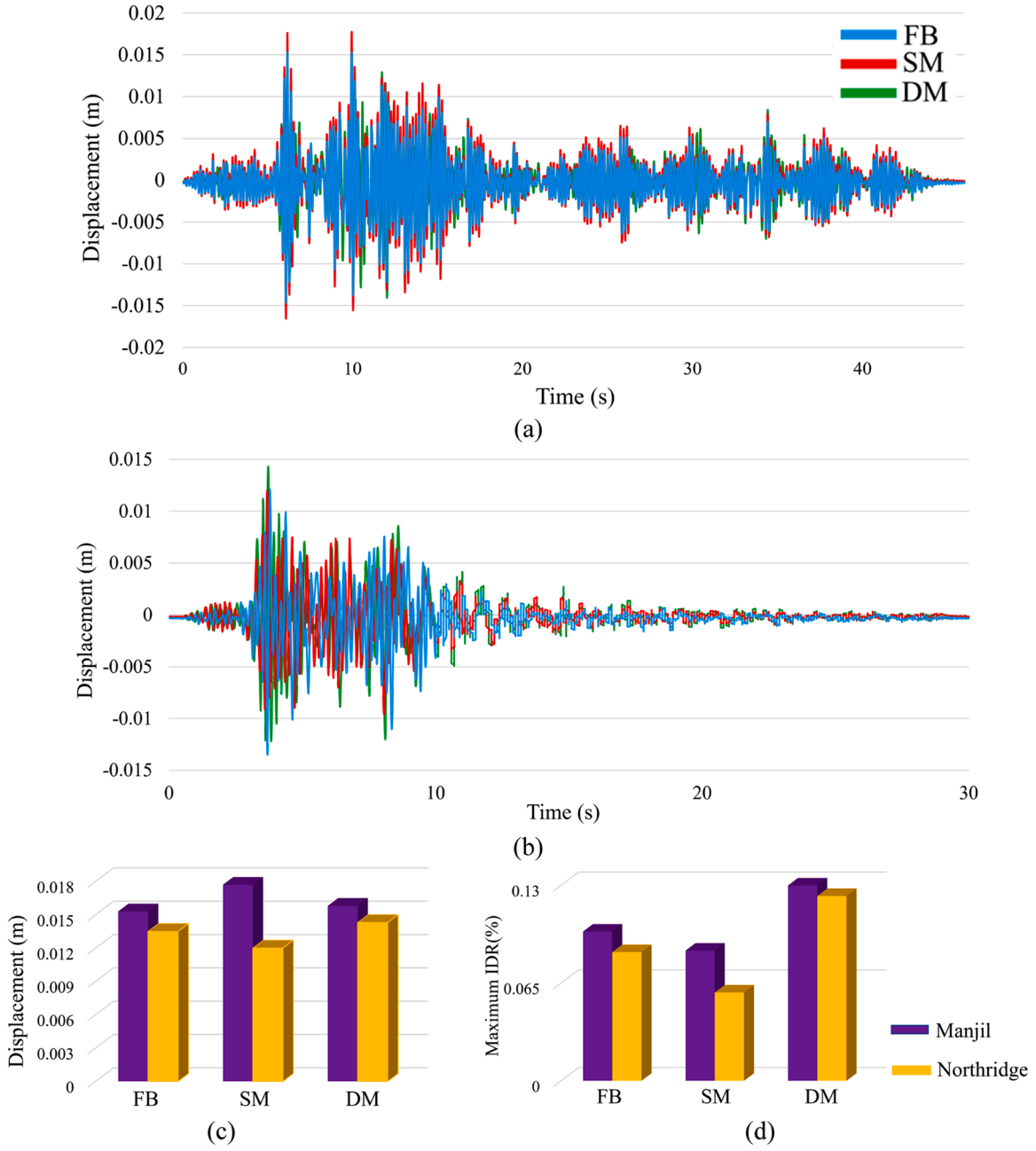

Fig. 16. Top displacement versus time plot for (a) Manjil, and (b) Northridge seismic records' analyses, (c) top displacement and (c) maximum IDR values of the models for two seismic records' analyses.

8. Conclusion

A framework for developing digital twins of the cultural heritage assets is proposed using 3D laser scanners and accelerometer sensors, and its application is investigated on a case study called Slottsfjell tower in Tønsberg, Norway. Geometrical survey of the tower was conducted using 3D laser scanners and a semi-automatic procedure for converting the point clouds to the FEM is presented in this study. Afterward, system identification of the tower was carried out by performing AVT and OMA. Three different frequency domain OMA techniques were utilized to define the natural frequencies and corresponding mode shapes of the tower. Since destructive tests are not allowed on cultural heritage assets, vibration-based FEM updating is done to investigate the material properties of different parts of the tower. Mechanical properties of the tønsbergite stone were utilized to derive the base values of the material properties of the homogenized masonry for performing the FEM updating. To investigate the influence of the SSI on the FEM updating results, three FEMs were developed. In the FB model, the SSI was neglected by considering rigid boundary conditions, the SM model was developed by modeling triaxial springs beneath the structure and the DM model was generated by modeling the foundation and soil box using the direct method. Firstly, a sensitivity analysis was performed on the three developed FEMs so that E_z, G_{xz}, G_{yz} are the most effective parameters effective on the frequency values. Unlike E_z, which is effective on the first two modes, G_{xz} and G_{yz} are effective on higher modes. Properties of soil are not as effective as the masonry properties in the DM model, but in the SM model, soil spring stiffnesses are considered as the most effective parameters. After performing FEM updating of the models, ADFVs and MAC values show that the FB model is paired with the test results on the first two modes. By considering the SSI effects in the SM model, the ADFVs and MAC values enhanced for the higher modes, and in the DM model as the most detailed model, the correlation is improved. The DM model is considered as the closest model to the real structure in terms of the frequency values and mode shapes. Moreover, it is investigated that updated material properties of the FB model are conservative compared to the other two models that SSI effects are considered. Fundamental periods of soil and structure are computed for the DM model separately that are not close to each other. It confirms that the tower is not at the risk of resonance effect. Furthermore, linear time history analyses were carried out by applying two strong ground motions. The results show negligible differences in term of the top displacement, but the maximum IDR values of DM model are more than the other two models. Although, it is tried to calibrate the models based on the OMA results, and the updated material properties of the FB model are conservative, the larger values of maximum IDR are concluded from dynamic analyses of DM model. SSI is effective on the dynamic response of structures that can facilitate the FEM updating procedure to obtain reliable enough FEMs for performing vulnerability assessments. Nonlinear time history analyses using various seismic records with different characteristics as well as performing in-situ tests on soil layers' material properties are still needed to be done to evaluate the reliability of various SSI modeling approaches.

Declaration of Competing Interest

The authors declare that they have no known competing financial interests or personal relationships that could have appeared to influence the work reported in this paper.

Acknowledgements

This work is a part of the HYPERION project. HYPERION has received funding from the European Union's Framework Programme for Research and Innovation (Horizon 2020) under Grant agreement no. 821054. The contents of this publication are the sole responsibility of Oslo Metropolitan University (Work Package 5, Task 2) and do not necessarily reflect the opinion of the European Union.

References

[1] F.J. Pallarés, M. Betti, G. Bartoli, L. Pallarés, Structural health monitoring (SHM) and Nondestructive testing (NDT) of slender masonry structures: a practical review, Constr. Build. Mater. 297 (2021), 123768, https://doi.org/10.1016/j.conbuildmat.2021.123768.
[2] A. Shabani, M. Kioumarsi, V. Plevris, H. Stamatopoulos, Structural vulnerability assessment of heritage timber buildings: a methodological proposal, Forests 11 (8) (2020) 881, https://doi.org/10.3390/f11080881.
[3] G. Standoli, E. Giordano, G. Milani, F. Clementi, Model updating of historical belfries based on oma identification techniques, Int. J. Archit. Herit. 15 (1) (2021) 132–156, https://doi.org/10.1080/15583058.2020.1723735.
[4] A. Shabani, M. Kioumarsi, M. Zucconi, State of the art of simplified analytical methods for seismic vulnerability assessment of unreinforced masonry buildings, Eng. Struct. 239 (2021), 112280, https://doi.org/10.1016/j.engstruct.2021.112280.
[5] G. Angjeliu, D. Coronelli, G. Cardani, Development of the simulation model for Digital Twin applications in historical masonry buildings: the integration between numerical and experimental reality, Comput. Struct. 238 (2020), 106282, https://doi.org/10.1016/j.compstruc.2020.106282.
[6] M. Korumaz, M. Betti, A. Conti, G. Tucci, G. Bartoli, V. Bonora, A.G. Korumaz, L. Fiorini, An integrated Terrestrial Laser Scanner (TLS), Deviation Analysis (DA) and Finite Element (FE) approach for health assessment of historical structures. A minaret case study, Eng. Struct. 153 (2017) 224–238, https://doi.org/10.1016/j.engstruct.2017.10.026.
[7] R.S. Panah, M. Kioumarsi, Application of building information modelling (BIM) in the health monitoring and maintenance process: a systematic review, Sensors 21 (3) (2021) 837, https://doi.org/10.3390/s21030837.
[8] G. Castellazzi, A.M. D'Altri, S. de Miranda, F. Ubertini, An innovative numerical modeling strategy for the structural analysis of historical monumental buildings, Eng. Struct. 132 (2017) 229–248, https://doi.org/10.1016/j.engstruct.2016.11.032.
[9] D.F. Laefer, L. Truong-Hong, Toward automatic generation of 3D steel structures for building information modelling, Autom. Constr. 74 (2017) 66–77, https://doi.org/10.1016/j.autcon.2016.11.011.
[10] L. Barazzetti, F. Banfi, R. Brumana, G. Gusmeroli, D. Oreni, M. Previtali, F. Roncoroni, G. Schiantarelli, BIM from laser clouds and finite element analysis: combining structural analysis and geometric complexity, ISPRS – International Archives of the Photogrammetry, Remote Sensing and Spatial Information Sciences XL-5/W4, 2015, pp. 345–50. ⟨http://dx.doi.org/10.5194/isprsarchives-XL-5-W4-345-2015⟩.

[11] G. Castellazzi, A.M. Altri, G. Bitelli, I. Selvaggi, A. Lambertini, From laser scanning to finite element analysis of complex buildings by using a semi-automatic procedure, Sensors 15 (8) (2015) 18360–18380, https://doi.org/10.3390/s150818360.
[12] G. Bartoli, M. Betti, V. Bonora, A. Conti, L. Fiorini, V.C. Kovacevic, V. Tesi, G. Tucci, From TLS data to FE model: a workflow for studying the dynamic behavior of the Pulpit by Giovanni Pisano in Pistoia (Italy), Procedia Struct. Integr. 29 (2020) 55–62, https://doi.org/10.1016/j.prostr.2020.11.139.
[13] C. Pepi, N. Cavalagli, V. Gusella, M. Gioffrè, An integrated approach for the numerical modeling of severely damaged historic structures: application to a masonry bridge, Adv. Eng. Softw. 151 (2021), 102935, https://doi.org/10.1016/j.advengsoft.2020.102935.
[14] N. Kassotakis, V. Sarhosis, Employing non-contact sensing techniques for improving efficiency and automation in numerical modelling of existing masonry structures: a critical literature review, Structures 32 (2021) 1777–1797, https://doi.org/10.1016/j.istruc.2021.03.111.
[15] S.L. Kramer, Geotechnical Earthquake Engineering, Pearson Education India, 1996.
[16] A. Shabani, A. Alinejad, M. Teymouri, A.N. Costa, M. Shabani, M. Kioumarsi, Seismic vulnerability assessment and strengthening of heritage timber buildings: a review, Buildings 11 (12) (2021) 661, https://doi.org/10.3390/buildings11120661.
[17] A. Fathi, A. Sadeghi, M.R. Emami Azadi, N. Hoveidaie, Assessing seismic behavior of a masonry historic building considering soil-foundation-structure interaction (case study of Arge-Tabriz), Int. J. Archit. Herit. 14 (6) (2020) 795–810, https://doi.org/10.1080/15583058.2019.1568615.
[18] V. Anand, S.R. Satish Kumar, Seismic soil-structure interaction: a state-of-the-art review, Structures 16 (2018) 317–326, https://doi.org/10.1016/j.istruc.2018.10.009.
[19] F. de Silva, F. Ceroni, S. Sica, F. Silvestri, Non-linear analysis of the Carmine bell tower under seismic actions accounting for soil–foundation–structure interaction, Bull. Earthq. Eng. 16 (7) (2018) 2775–2808, https://doi.org/10.1007/s10518-017-0298-0.
[20] A. Mortezaei, A. Motaghi, Seismic assessment of the world's tallest pure-brick tower including soil-structure interaction, J. Perform. Constr. Facil. 30 (5) (2016), 04016020, https://doi.org/10.1061/(ASCE)CF.1943-5509.0000861.
[21] E. Hökelekli, A. Al-Helwani, Effect of soil properties on the seismic damage assessment of historical masonry minaret–soil interaction systems, Struct. Des. Tall Spec. Build. 29 (2) (2020), e1694, https://doi.org/10.1002/tal.1694.
[22] Y.S. Erdogan, Discrete and continuous finite element models and their calibration via vibration and material tests for the seismic assessment of masonry structures, Int. J. Archit. Herit. 11 (7) (2017) 1026–1045, https://doi.org/10.1080/15583058.2017.1332255.
[23] A. Drougkas, E. Verstrynge, P. Szekér, G. Heirman, L.-E. Bejarano-Urrego, G. Giardina, K. Van Balen, Numerical modeling of a church nave wall subjected to differential settlements: soil-structure interaction, time-dependence and sensitivity analysis, Int. J. Archit. Herit. 14 (8) (2020) 1221–1238, https://doi.org/10.1080/15583058.2019.1602682.
[24] A. Rahmani, M. Taiebat, W.D. Liam Finn, C.E. Ventura, Evaluation of substructuring method for seismic soil-structure interaction analysis of bridges, Soil Dyn. Earthq. Eng. 90 (2016) 112–127, https://doi.org/10.1016/j.soildyn.2016.08.013.
[25] R. Mario Azzara, G. De Roeck, M. Girardi, C. Padovani, D. Pellegrini, E. Reynders, The influence of environmental parameters on the dynamic behaviour of the San Frediano bell tower in Lucca, Eng. Struct. 156 (2018) 175–187, https://doi.org/10.1016/j.engstruct.2017.10.045.
[26] P. Barsocchi, G. Bartoli, M. Betti, M. Girardi, S. Mammolito, D. Pellegrini, G. Zini, Wireless sensor networks for continuous structural health monitoring of historic masonry towers, Int. J. Archit. Herit. 15 (1) (2021) 22–44, https://doi.org/10.1080/15583058.2020.1719229.
[27] A. Bayraktar, İ. Çalik, T. Türker, A. Ashour, Restoration effects on experimental dynamic characteristics of masonry stone minarets, Mater. Struct. 51 (6) (2018) 141, https://doi.org/10.1617/s11527-018-1272-2.
[28] D. Bru, S. Ivorra, M. Betti, J.M. Adam, G. Bartoli, Parametric dynamic interaction assessment between bells and supporting slender masonry tower, Mech. Syst. Signal Process. 129 (2019) 235–249, https://doi.org/10.1016/j.ymssp.2019.04.038.
[29] C. Castagnetti, E. Bassoli, L. Vincenzi, F. Mancini, Dynamic assessment of masonry towers based on terrestrial radar interferometer and accelerometers, Sensors 19 (6) (2019) 1319, https://doi.org/10.3390/s19061319.
[30] B. Erdil, M. Tapan, İ. Akkaya, F. Korkut, Effects of structural parameters on seismic behaviour of historical masonry minaret, Period. Polytech. Civ. Eng. 62 (1) (2018) 148–161, https://doi.org/10.3311/PPci.10687.
[31] R.M. Azzara, M. Girardi, V. Iafolla, C. Padovani, D. Pellegrini, Long-term dynamic monitoring of medieval masonry towers, Front. Built Environ. 6 (9) (2020), https://doi.org/10.3389/fbuil.2020.00009.
[32] F. Ubertini, G. Comanducci, N. Cavalagli, Vibration-based structural health monitoring of a historic bell-tower using output-only measurements and multivariate statistical analysis, Struct. Health Monit. 15 (4) (2016) 438–457, https://doi.org/10.1177%2F1475921716643948.
[33] A. D'Ambrisi, V. Mariani, M. Mezzi, Seismic assessment of a historical masonry tower with nonlinear static and dynamic analyses tuned on ambient vibration tests, Eng. Struct. 36 (2012) 210–219, https://doi.org/10.1016/j.engstruct.2011.12.009.
[34] I. Capanna, R. Cirella, A. Aloisio, R. Alaggio, F. Di Fabio, M. Fragiacomo, Operational modal analysis, model update and fragility curves estimation, through truncated incremental dynamic analysis, of a masonry belfry, Buildings 11 (3) (2021) 120, https://doi.org/10.3390/buildings11030120.
[35] E. García-Macías, L. Ierimonti, I. Venanzi, F. Ubertini, An innovative methodology for online surrogate-based model updating of historic buildings using monitoring data, Int. J. Archit. Herit. 15 (1) (2021) 92–112, https://doi.org/10.1080/15583058.2019.1668495.
[36] C. Gentile, A. Saisi, A. Cabboi, Structural identification of a masonry tower based on operational modal analysis, Int. J. Archit. Herit. 9 (2) (2015) 98–110, https://doi.org/10.1080/15583058.2014.951792.
[37] G. Lacanna, M. Betti, M. Ripepe, G. Bartoli, Dynamic identification as a tool to constrain numerical models for structural analysis of historical buildings, Front. Built Environ. 6 (40) (2020), https://doi.org/10.3389/fbuil.2020.00040.
[38] A.C. Altunişik, A.F. Genç, M. Günaydin, F.Y. Okur, O.Ş. Karahasan, Dynamic response of a historical armory building using the finite element model validated by the ambient vibration test, J. Vib. Control 24 (22) (2018) 5472–5484, https://doi.org/10.1177%2F1077546318755559.
[39] E. Bassoli, L. Vincenzi, A.M. D'Altri, S. de Miranda, M. Forghieri, G. Castellazzi, Ambient vibration-based finite element model updating of an earthquake-damaged masonry tower, Struct. Control Health Monit. 25 (5) (2018), e2150, https://doi.org/10.1002/stc.2150.
[40] R. Lancellotta, D. Sabia, Identification technique for soil-structure analysis of the Ghirlandina Tower, Int. J. Archit. Herit. 9 (4) (2015) 391–407, https://doi.org/10.1080/15583058.2013.793438.
[41] M. Ferraioli, L. Miccoli, D. Abruzzese, A. Mandara, Dynamic characterisation and seismic assessment of medieval masonry towers, Nat. Hazards 86 (2) (2017) 489–515, https://doi.org/10.1007/s11069-016-2519-2.
[42] L.F. Ramos, L. Marques, P.B. Lourenço, G. De Roeck, A. Campos-Costa, J. Roque, Monitoring historical masonry structures with operational modal analysis: two case studies, Mech. Syst. Signal Process. 24 (5) (2010) 1291–1305, https://doi.org/10.1016/j.ymssp.2010.01.011.
[43] F. Ceroni, S. Sica, M. Rosaria Pecce, A. Garofano, Evaluation of the natural vibration frequencies of a historical masonry building accounting for SSI, Soil Dyn. Earthq. Eng. 64 (2014) 95–101, https://doi.org/10.1016/j.soildyn.2014.05.003.
[44] A. Karatzetzou, D. Pitilakis, S. Karafagka, System identification of mosques resting on soft soil. the case of the Suleiman mosque in the Medieval City of Rhodes, Greece, Geosciences 11 (7) (2021) 275, https://doi.org/10.3390/geosciences11070275.
[45] S. Gönen, S. Soyöz, Seismic analysis of a masonry arch bridge using multiple methodologies, Eng. Struct. 226 (2021), 111354, https://doi.org/10.1016/j.engstruct.2020.111354.
[46] K. Demirlioglu, S. Gonen, S. Soyoz, M.P. Limongelli, In-plane seismic response analyses of a historical brick masonry building using equivalent frame and 3D FEM modeling approaches, Int. J. Archit. Herit. 14 (2) (2020) 238–256, https://doi.org/10.1080/15583058.2018.1529208.
[47] H. Güllü, F. Özel, Microtremor measurements and 3D dynamic soil–structure interaction analysis for a historical masonry arch bridge under the effects of near- and far-fault earthquakes, Environ. Earth Sci. 79 (13) (2020) 338, https://doi.org/10.1007/s12665-020-09086-0.
[48] F. Ubertini, N. Cavalagli, A. Kita, G. Comanducci, Assessment of a monumental masonry bell-tower after 2016 Central Italy seismic sequence by long-term SHM, Bull. Earthq. Eng. 16 (2) (2018) 775–801, https://doi.org/10.1007/s10518-017-0222-7.
[49] H. Güllü, H.S. Jaf, Full 3D nonlinear time history analysis of dynamic soil–structure interaction for a historical masonry arch bridge, Environ. Earth Sci. 75 (21) (2016) 1421, https://doi.org/10.1007/s12665-016-6230-0.

[50] A. Shabani, M. Kioumarsi, A novel macroelement for seismic analysis of unreinforced masonry buildings based on MVLEM in OpenSees, J. Build. Eng. 49 (2022), 104019, https://doi.org/10.1016/j.jobe.2022.104019.
[51] A.M. Chandler, N.T.K. Lam, M.N. Sheikh, Response spectrum predictions for potential near-field and far-field earthquakes affecting Hong Kong: soil sites, Soil Dyn. Earthq. Eng. 22 (6) (2002) 419–440, https://doi.org/10.1016/S0267-7261(02)00041-6.
[52] N.T.K. Lam, J.L. Wilson, A.M. Chandler, Seismic displacement response spectrum estimated from the frame analogy soil amplification model, Eng. Struct. 23 (11) (2001) 1437–1452, https://doi.org/10.1016/S0141-0296(01)00049-9.
[53] H. Güllü, M. Pala, On the resonance effect by dynamic soil–structure interaction: a revelation study, Nat. Hazards 72 (2) (2014) 827–847, https://doi.org/10.1007/s11069-014-1039-1.
[54] M. Tolun, B. Emirler, A. Yildiz, H. Güllü, Dynamic response of a single pile embedded in sand including the effect of resonance, Period. Polytech. Civ. Eng. 64 (4) (2020) 1038–1050, https://doi.org/10.3311/PPci.15027.
[55] ReCap, Autodesk ReCap Pro, California, U.S, 2021.
[56] Revit, Autodesk Revit BIM (Building Information Modeling), California, U.S, 2021.
[57] DIANA, Diana User's Manual, Release 10.4, DIANA FEA BV, Delft University of Technology, Netherland, 2020.
[58] M.A. Adam, T.S. El-Salakawy, M.A. Salama, A.A. Mohamed, Assessment of structural condition of a historic masonry minaret in Egypt, Case Stud. Constr. Mater. 13 (2020), e00409, https://doi.org/10.1016/j.cscm.2020.e00409.
[59] K.V. Katakalos, I.A. Arnaoutis, G.C. Manos, Identification of failure mechanism of the ottoman bath (hamam) at apollonia (pazarouda) exploiatation of historical data, Case Stud. Constr. Mater. 14 (2021), e00475, https://doi.org/10.1016/j.cscm.2020.e00475.
[60] A. Shabani, S. Erfani, Seismic performance evaluation of SSMF with simple beam–column connections under the base level, Int. J. Steel Struct. 20 (1) (2020) 89–100, https://doi.org/10.1007/s13296-019-00273-9.
[61] E. Winkler, Die Lehre von der Elasticitaet und Festigkeit: mit besonderer Rücksicht auf ihre Anwendung in der Technik, für polytechnische Schulen, Bauakademien, Ingenieure, Maschinenbauer, Architecten, etc, H. Dominicus, 1867.
[62] M. Choinière, P. Paultre, P. Léger, Influence of soil-structure interaction on seismic demands in shear wall building gravity load frames, Eng. Struct. 198 (2019), 109259, https://doi.org/10.1016/j.engstruct.2019.05.100.
[63] C. Yoo, Interaction between tunneling and bridge foundation – a 3D numerical investigation, Comput. Geotech. 49 (2013) 70–78, https://doi.org/10.1016/j.compgeo.2012.11.005.
[64] Dynamic Design Solutions, FEMtools 4, Leuven, Belgium, 2021.
[65] I.T. Rosenqvist, Electron-microscope investigations of larvikite and tönsbergite feldspars, Nor. Geol. Tidsskr. 45 (1) (1965) 69–71.
[66] A. Ademi, Finite Element Model Updating of A Stone Masonry Tower Using 3D Laser Scanner and Accelerometers, Department of Civil Engineering and Energy Technology, Oslo Metropolitan University, Oslo, Norway, 2020.
[67] J.S. Petersen, Structure of the larvikite-lardalite complex, Oslo-region, Norway, and its evolution, Geol. Rundsch. 67 (1) (1978) 330–342.
[68] A. Palmström, R. Singh, The deformation modulus of rock masses—comparisons between in situ tests and indirect estimates, Tunn. Undergr. Space Technol. 16 (2) (2001) 115–131, https://doi.org/10.1016/S0886-7798(01)00038-4.
[69] B. Ghiassi, A.T. Vermelfoort, P.B. Lourenço, Chapter 7 – masonry mechanical properties, in: B. Ghiassi, G. Milani (Eds.), Numerical Modeling of Masonry and Historical Structures, Woodhead Publishing, 2019, pp. 239–261, https://doi.org/10.1016/B978-0-08-102439-3.00007-5.
[70] R. Zavalis, B. Jonaitis, P.B. Lourenço, Analysis of bed joint influence on masonry modulus of elasticity, in: Proceedings of the 9th International Masonry Conference 2014, Guimarães, Portugal, 2014.
[71] P. Croce, M.L. Beconcini, P. Formichi, P. Cioni, F. Landi, C. Mochi, F. De Lellis, E. Mariotti, I. Serra, Shear modulus of masonry walls: a critical review, Procedia Struct. Integr. 11 (2018) 339–346, https://doi.org/10.1016/j.prostr.2018.11.044.
[72] A.B. Vesić, Bending of beams resting on isotropic elastic solid, J. Eng. Mech. Div. 87 (2) (1961) 35–53.
[73] L.R. Herrmann, Finite element analysis of contact problems, J. Eng. Mech. Div. 104 (5) (1978) 1043–1057.
[74] S. Shamloo, M. Imani, Subgrade reaction modulus of rock masses under the load of single and multiple footings, Geomech. Geoengin. (2021) 1–19, https://doi.org/10.1080/17486025.2021.1889687.
[75] R. Ribeiro, R. Lameiras, Evaluation of low-cost MEMS accelerometers for SHM: frequency and damping identification of civil structures, Lat. Am. J. Solids Struct. 16 (2019) 203, https://doi.org/10.1590/1679-78255308.
[76] A. Shabani, A. Ademi, M. Kioumarsi, Structural Model Updating of a Historical Stone Masonry Tower in Tønsberg, Norway, Springer International Publishing, Cham, 2022, pp. 576–585, https://doi.org/10.1007/978-3-030-90788-4_45.
[77] F.B. Zahid, Z.C. Ong, S.Y. Khoo, A review of operational modal analysis techniques for in-service modal identification, J. Braz. Soc. Mech. Sci. Eng. 42 (8) (2020) 398, https://doi.org/10.1007/s40430-020-02470-8.
[78] R. Brincker, C. Ventura, Introduction to Operational Modal Analysis, John Wiley & Sons, 2015.
[79] N.-J. Jacobsen, P. Andersen, R. Brincker, Applications of frequency domain curve-fitting in the EFDD technique, in: Conference Proceedings: IMAC-XXVI: A Conference & Exposition on Structural Dynamics, Society for Experimental Mechanics, 2008.
[80] M. Masjedian, M. Keshmiri, A review on operational modal analysis researches: classification of methods and applications, in: Proceedings of the 3rd IOMAC, 2009, pp. 707–18.
[81] SVIBS, ARTeMIS Modal, Structural Vibration Solution, Aalborg, Denmark, 2021.
[82] P.B. Schnabel, SHAKE: A Computer Program for Earthquake Response Analysis of Horizontally Layered Sites (EERC Report 72-12), University of California, Berkeley, 1972.
[83] V. Silva, D. Amo-Oduro, A. Calderon, J. Dabbeek, V. Despotaki, L. Martins, A. Rao, M. Simionato, D. Viganò, C. Yepes, Global earthquake model (GEM) seismic risk map (version 2018.1), 2018.
[84] PEER, PEER ground motion database, NGA West2, 2014. (Accessed 18 January 2022).
[85] H. Güllü, M. Karabekmez, Effect of near-fault and far-fault earthquakes on a historical masonry mosque through 3D dynamic soil-structure interaction, Eng. Struct. 152 (2017) 465–492, https://doi.org/10.1016/j.engstruct.2017.09.031.
[86] B. Borzi, H. Crowley, R. Pinho, Simplified pushover-based earthquake loss assessment (SP-BELA) method for masonry buildings, Int. J. Archit. Herit. 2 (4) (2008) 353–376, https://doi.org/10.1080/15583050701828178.